A semianalytic radio frequency sheath model integrated into a two-dimensional hybrid model for plasma processing reactors

Michael J. Grapperhaus[a] and Mark J. Kushner[b]
University of Illinois, 1406 W. Green Street, Urbana, Illinois 61801

(Received 23 July 1996; accepted for publication 9 October 1996)

In high plasma density ($[e]>10^{11}-10^{12}$ cm^{-3}) reactors for materials processing, the sheath thickness is often <100 s μm while the reactor dimensions are 10 s cm. Resolving the sheath in computer models of these devices using reasonable grid resolution is therefore problematic. If the sheath is not resolved, the plasma potential and stochastic electron heating produced by the substrate bias may not be well represented. In this article, we describe a semianalytic model for radio frequency (rf) biased sheaths which has been integrated into a two-dimensional model for plasma etching reactors. The basis of the sheath model is to track the charging and discharging of the sheath in time, and use a one-dimensional analytical model to obtain the instantaneous sheath voltage drop based on the sheath charge and the plasma conditions at the sheath edge. Results from the integrated model for an inductively coupled plasma etching reactor with powers of 200–800 W and rf bias powers from 50 to 400 W in Ar and Ar/Cl_2 will be discussed. We found that the sheath voltage wave form remains nearly sinusoidal, and that the plasma density, and consequently the ion flux to the surface, scale primarily with inductively coupled power. © *1997 American Institute of Physics.*
[S0021-8979(97)04602-1]

I. INTRODUCTION

High plasma density plasma ($[e]>10^{11}-10^{12}$ cm^{-3}) etching reactors have become important tools in the fabrication of <0.5 μm features in microelectronics devices. Low pressure-high plasma density sources produce more anisotropic etching than traditional parallel plate reactive ion etchers due to the low collisionality of the ions across the thin sheaths obtained in these reactors. Inductively coupled plasma (ICP) reactors are one high plasma density tool which provide uniform plasma properties across a large substrate. By using ICP tools, one has the ability to independently vary the applied substrate voltage and the inductively coupled power with the intent to have independent control of ion energies and ion fluxes.[1–6] Previous works have shown that plasma density and ion energies are interdependent, but that the desired operating conditions can usually be achieved by the proper combination of inductively coupled power and substrate bias voltage.[3,4]

In the modeling of plasma etching equipment which have radio frequency (rf) biases on the substrate, the rf sheath must be accurately represented to properly simulate the ambipolar fields, electron stochastic heating, and the dc bias. In high plasma density reactors, the rf sheath width may be <100 s μm whereas reactor dimensions are 10 s cm.[7–10] Numerically resolving the thin sheath in computer models of these devices therefore requires large computing resources and, in many cases, is impractical. Much progress has been made in developing semianalytical solutions for rf sheaths as encountered in plasma etching reactors.[7–14] Since, however, these semianalytical models typically require *a priori* knowledge of the bulk plasma conditions, they must be integrated with plasma equipment models to be applied to the conditions of interest.

Several sheath models have been developed in recent years, among them Lieberman,[7,11] Metze, Ernie, and Oskam (MEO),[12] and Riley.[13] The Lieberman model assumes that the electrons are sufficiently cold and are excluded from the sheath, and that the ions see only the time averaged potential, which is essentially the high frequency limit. The MEO model allows electrons to have a temperature, but assumes that the ions respond to the instantaneous sheath voltage, which is the low frequency limit. The unified sheath model developed by Riley is an attempt to bridge the frequency range between the Lieberman and MEO models. It assumes that the ions move in a time damped or averaged potential governed by a relaxation time, τ_r, which is approximately the ion transit time across the sheath.

Sheath models typically require the bulk plasma properties as input and so must make assumptions about the bulk plasma conditions. These assumptions include the time dependence of the total current through the sheath, and boundary conditions for the electric field at the sheath edge, which is typically assumed to be zero. Since boundary conditions for the sheath have been shown to have an important effect on the sheath voltage and current,[8,9,15,16] sheath models should ultimately be integrated with the solution of the bulk plasma conditions in a self-consistent fashion.[17]

To address these issues, we have developed a sheath model which is solved self-consistently within the framework of a two-dimensional plasma equipment model.[6] In high plasma density reactors, the sheath is thin compared to the dimensions of interest and so the sheath locally appears to be one-dimensional. The sheath model (SM) we developed takes advantage of this scaling. The SM consists of a one-dimensional local model which is implemented at each mesh point at the boundary of the plasma and the walls of the reactor. The SM tracks the charging and discharging of

[a]Department of Nuclear Engineering. Electronic mail: grapper@uiuc.edu
[b]Department of Electrical and Computer Engineering: Electronic mail: mjk@uiuc.edu

 0021-8979/97/81(2)/569/9/$10.00 © 1997 American Institute of Physics

the sheath during the rf cycle by integrating, in time, the electron and ion currents into and out of the sheath. Ions are assumed to collisionlessly traverse the sheath in a time damped potential as in the Riley model.[13] It is also assumed that the electrons within the sheath can be described by a Boltzmann distribution. The charged particle profiles in the sheath are then known and Poisson's equation can be integrated to determine the sheath voltage drop at a given location at the boundary of the plasma and specified point in time. The sheath voltage drop is then applied as a jump condition in the solution of Poisson's equation in the entire reactor.

In Sec. II, the SM is described in the context of incorporating it into a two-dimensional hybrid plasma model for an ICP etching tool. In Section III, validation of the dc portion of the sheath model is discussed. Plasma properties obtained with and without the SM will be compared and described in Sec. IV. Plasmas will be examined having inductively coupled powers from 200 to 800 W and rf bias powers from 50 to 400 W for Ar and Ar/Cl_2 gas mixtures. We found that the sheath voltage wave form remains nearly sinusoidal, and that the plasma density, and consequently the ion flux to the surface, scale primarily with inductively coupled power. Concluding remarks are in Sec. V.

II. DESCRIPTION OF THE MODEL

The plasma model we have used in this study has been previously discussed, therefore, it will be only briefly described here.[6] The simulation, called the hybrid plasma equipment model (HPEM) is a two-dimensional model consisting of an electromagnetic module (EMM), an electron Monte Carlo simulation (EMCS), and a fluid-chemical kinetics simulation (FKS). The inductively coupled electromagnetic fields are produced by the EMM. Those fields are used in the EMCS to generate the electron energy distribution as a function of position and phase. These distributions are then used to produce electron transport coefficients and electron impact source functions. These values are transferred to the FKS in which the continuity and momentum equations for all heavy charged and neutral species are solved, and Poisson's equation is solved for the electrostatic fields. A drift diffusion formulation is used for the electrons to enable an implicit solution of Poisson's equation. The densities, conductivity, and fields obtained from the FKS are then transferred to the EMM and EMCS. This iterative cycle is repeated until a converged solution is obtained.

The version of the HPEM used here also incorporates an equivalent circuit model for the coil and matchbox to provide coil currents and voltages. These values are used as boundary conditions in solution of Maxwell's equations (in the EMM) and Poisson's equation (in the FKS), respectively. The details of the coil circuit and manner of coupling to the plasma and electromagnetics model are discussed in Ref. 18. The coil is interfaced to the rf generator by a matchbox. The circuit model varies matchbox capacitor values (parallel and series) to minimize the reflected power from the plasma. The generator voltage is simultaneously adjusted to deliver the desired inductively coupled power to the plasma.

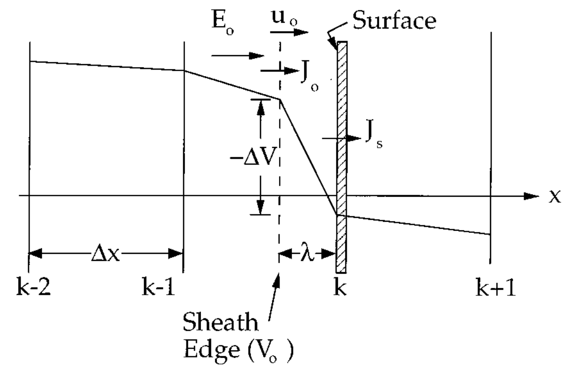

FIG. 1. Schematic of the sheath model geometry. Values at the sheath edge are denoted by the subscript ''0'' and values at the surface of the wall by the subscript ''s.''

The SM is implemented in the HPEM in the following manner. The plasma properties in the last computational plasma cell adjacent to a wall in the reactor are schematically shown in Fig. 1. Particle densities and potentials are solved for the vertice points (and on surfaces) denoted by $k \pm \ell$, where k is the mesh point on the surface of the wall. Quantities at the sheath edge are denoted by a subscript ''0'' and quantities at the surface of the wall are denoted by a subscript ''s.'' We assume that the sheath is one-dimensional and has a thickness, λ, smaller than the grid resolution defined by the cell width, Δx. Using a finite difference approximation, the electric field above the sheath, E_0, is given by:

$$E_0 = -\frac{V_0 - V_{k-1}}{\Delta x - \lambda}, \tag{1}$$

where V_0 is the potential at the sheath edge and V_{k-1} is the potential at the last node in the plasma. Since typically $\lambda \ll \Delta x$ then $\Delta x - \lambda \approx \Delta x$. The electric field at the surface, E_s, is then given by Gauss' law,

$$E_s = E_0 + \frac{Q}{\varepsilon_0}, \tag{2}$$

where Q is the charge density (coulombs/cm^2) contained in the sheath.

The time rate of change of the sheath charge density, Q, can be obtained from the charged particle currents into and out of the sheath:

$$\frac{dQ}{dt} = (j_{e_0} - j_{e_s}) + \sum_i (j_{i_0} - j_{i_s}), \tag{3}$$

where j_e is the electron current and j_i is the ion current from ion species i. In the results we present here, we assumed that there are no negative ion species in the sheath region, since for our conditions, negative ions are well isolated from the sheath nearer the center of the plasma where the plasma potential is most positive.[19] The model will, however, handle negative particles should they penetrate the sheath as long as their contribution to the space charge within the sheath is negligible. We also assume that $j_{i_0} \approx j_{i_s}$ which is a consequence of the steady state ion continuity equation. This expression is exact when the ions see only the time averaged potential, or when the ion transit time is much shorter than

the time scales of interest, in this case the rf period. Within the sheath, the electrons are assumed to have a Boltzmann distribution,

$$n_e(x)=n_{e_0}\exp\left(\frac{q[V(x)-V_0]}{kT_e}\right), \tag{4}$$

where k is Boltzmann's constant, T_e is the electron temperature, and $V(x)$ is the local potential. The electron current reaching the surface is

$$j_{e_s}=j_{e_0}\exp\left(\frac{q\Delta V}{kT_e}\right), \tag{5}$$

where $\Delta V=V_s-V_0$ is the voltage drop across the sheath. The electron temperature in the sheath is assumed to be the same as at the sheath edge, and is provided by the HPEM. E_0, n_{e_0}, j_{e_0}, and j_{i_0}, are also provided by the HPEM at each location along the wall.

The sheath charge density, Q, can now be tracked as a function of time provided that the sheath voltage drop can be related to the plasma properties and Q. This is the point where the one-dimensional model of the sheath is incorporated into the equipment model. Any model which properly represents the physics of the sheath and can relate the defined plasma properties and Q to the voltage drop can now be applied. The model used here is based on the unified sheath model of Riley.[13] The inclusion of multiple ion species is an extension.

The ions are assumed to move in a damped potential, $\bar{V}$. The ion continuity and energy equations are then used to determine the ion density in the sheath:

$$n_i(x)=n_{i_0}\left(1-\frac{2q\bar{V}(x)}{M_i u_{i_0}^2}\right)^{-1/2}, \tag{6}$$

where u_{i_0} is the larger of either the Bohm speed or the ion speed leaving the last plasma cell in the HPEM. The damped potential, $\bar{V}$, is computed from

$$\frac{d\bar{V}}{dt}=\frac{V-\bar{V}}{\tau_r}, \tag{7}$$

where τ_r is the ion relaxation time, approximated by the sheath thickness divided by the density averaged ion velocity entering the sheath. This formulation may slightly under estimate the transit time but is a reasonable approximation.

Using the charged species distributions [Eqs. (4) and (6)], Poisson's equation,

$$\frac{dE}{dx}=\frac{q}{\varepsilon_0}\left(\sum_i n_i-n_e\right) \tag{8}$$

is integrated across the sheath to yield the sheath voltage drop. In order to analytically integrate this equation, a relationship between the damped potential and the instantaneous potential must be known. Following the unified sheath model of Riley, we assumed that the damped potential has the same spatial distribution as the instantaneous voltage so that:

$$\bar{V}(x,t)\approx f(t)V(x,t). \tag{9}$$

The final expression for the first integral of the Poisson equation is then given by

$$\frac{1}{2}(E_s^2-E_0^2)=\frac{1}{\varepsilon_0}\left\{\sum_i n_{i_0}M_i u_{i_0}^2\left(\frac{\Delta V}{\Delta\bar{V}}\right)\left[\left(1-\frac{2q\Delta\bar{V}}{M_i u_{i_0}^2}\right)^{1/2}-1\right]+n_{e_0}kT_e\left[\exp\left(\frac{q\Delta V}{kT_e}\right)-1\right]\right\}. \tag{10}$$

Recall that E_s is related to E_0 and Q by Eq. (2). Therefore, Eqs. (2) and (10) provide implicit relations between the sheath charge, the plasma properties, and the voltage drop, which are solved by numerical iteration.

The sheath voltage drop is obtained at each wall location and at each time step during an rf cycle in the HPEM. The sheath properties are communicated back to the FKS by using ΔV as a jump condition in solving Poisson's equation. This is accomplished by assuming that the sheath thickness is much smaller than the grid spacing. In this case, by examining Fig. 1, the finite difference form of Poisson's equation at the last node above the sheath is

$$\frac{1}{\Delta x}\left[\left(\frac{V_0-V_{k-1}}{\Delta x}\right)-\left(\frac{V_{k-1}-V_{k-2}}{\Delta x}\right)\right]=-\frac{\rho_{k-1}}{\varepsilon_0}. \tag{11}$$

Recalling that $V_0=V_s-\Delta V$, yields a modified finite difference form for Poisson's equation,

$$\frac{1}{\Delta x}\left[\left(\frac{V_s-V_{k-1}}{\Delta x}\right)-\left(\frac{V_{k-1}-V_{k-2}}{\Delta x}\right)\right]=-\frac{\rho_{k-1}}{\varepsilon_0}+\frac{\Delta V}{(\Delta x)^2}. \tag{12}$$

If the wall is a conductor, then V_s is specified as a boundary condition. If the wall is a dielectric then, using Eq. (2), the finite difference form of Poisson's equation at the wall is

$$\frac{1}{\Delta x}\left[\varepsilon_r\left(\frac{V_1-V_s}{\Delta x}\right)-\left(\frac{V_s-V_{k-1}}{\Delta x}\right)\right]=-\frac{\rho_s}{\varepsilon_0}-\frac{Q}{\varepsilon_0\Delta x}-\frac{\Delta V}{(\Delta x)^2}. \tag{13}$$

In this way, Poisson's equation is solved in the same manner as when the analytic sheath is not used except that the additional terms on the right hand side (RHS) of Eqs. (12) and (13) are required in the last plasma cell and on dielectric walls, respectively.

In plasma models in which the sheath is not resolved, its effective thickness is at best the width of 1 numerical cell. The sheath will oscillate through this thickness during an rf cycle, which exaggerates its average speed by as much as the ratio $\Delta x/\lambda$. This exaggeration may cause artificially large stochastic heating of electrons since that heating rate is proportional to the sheath velocity. In the HPEM, the electron energy distribution is obtained in the EMCS which uses the time and spatially dependent electromagnetic fields (from the EMM) and electrostatic fields (from the FKS) to advance electron trajectories. To properly account for electron heating

at the rf sheath, the results of the SM must be incorporated into the EMCS. This is accomplished in the following manner.

In the EMCS, the sheath is also treated as being thin so that the transit time of the electrons across the sheath will be shorter than the time scale on which the sheath potential changes. The sheath thickness at a given time is approximated by the instantaneous sheath charge, Q, divided by the ion charge density at the sheath edge. This approximation will tend to under estimate the sheath thickness slightly, but is employed for practical purposes, since a numerical integration of the sheath charge distribution across the sheath at each surface point and at each time step would be too costly. An electron which reaches the sheath is checked to see if it has sufficiently large perpendicular component of velocity towards the wall to overcome the sheath potential and reach the wall. If so, the electron is collected. Electrons which can not overcome the sheath potential are reflected. In these cases, the electron velocity perpendicular to the wall is incremented by the sheath velocity. The sheath velocity is computed by a finite difference of the sheath thickness with respect to time, so that when the sheath is expanding, electrons leave with greater energy and when the sheath is collapsing, electrons leave with less energy. In this manner, stochastic electron heating by the rf sheath is properly taken into account.

III. VALIDATION

Before applying the SM to rf biased reactors, the dc characteristics of the SM were validated by comparing computed results for plasma potential, ion density, and electron temperature with electric probe measurements performed by Miller *et al.*[20] The measurements were made in the inductively coupled-gaseous electronics conference reference cell (IC-GECRC) for plasmas sustained in argon. The experimental technique and the IC-GECRC are described in detail in Ref. 20. Comparisons to experiments were performed at a pressure of 10 mTorr and power deposition up to 250 W.

The center line electron density, peak plasma potential, and electron temperature are shown in Fig. 2 as a function of power deposition with and without using the sheath model in the HPEM. The electron density, with and without the SM, and the reactor configuration, are shown in Fig. 3. In general, the cases using the SM agree better with the experiments. The plasma potential is both more positive and flatter as a function of axial position when using the SM. This results in an electron density which peaks on the centerline as observed experimentally. In many cases, the predicted plasma density without using the SM peaks off axis where the electron source function is the highest. (See Fig. 3.) This trend was also observed in the cases with an applied rf bias, and will be discussed in the next section. The electron temperature without the SM is somewhat higher than with the SM due to the lower plasma potential. This results in larger electron losses which requires a higher electron temperature (and electron source) to balance.

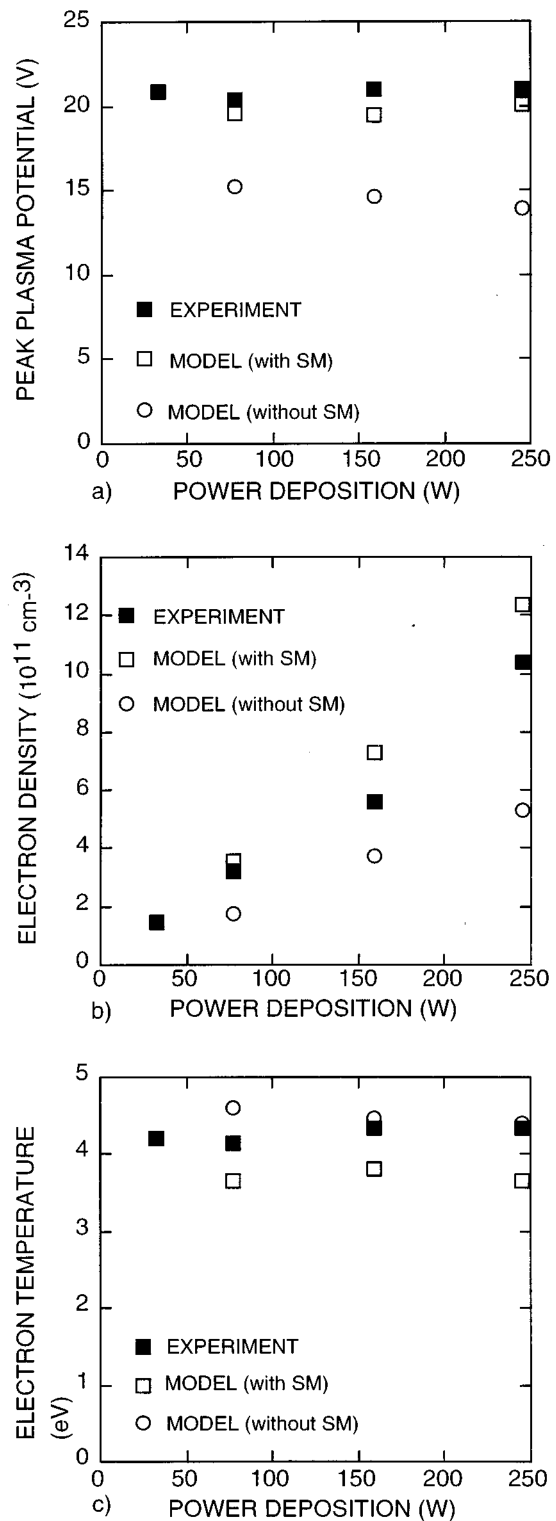

FIG. 2. Comparison of predicted plasma potential, electron density, and temperature with experiments (see Ref. 19). The gas is 10 mTorr Ar in the IC-GECRC. In general, the model using the SM agrees better with experiments.

IV. SHEATH PROPERTIES IN ICP ETCHING REACTORS

The demonstration geometry for this study is shown in Fig. 4 and is described in more detail in Ref. 6. The ICP reactor uses a flat spiral 4-turn coil set on top of a quartz

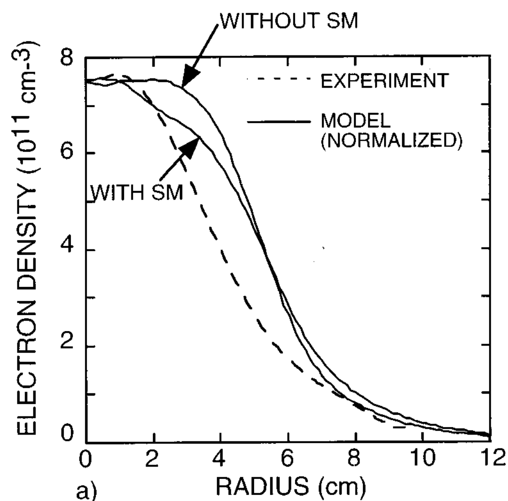

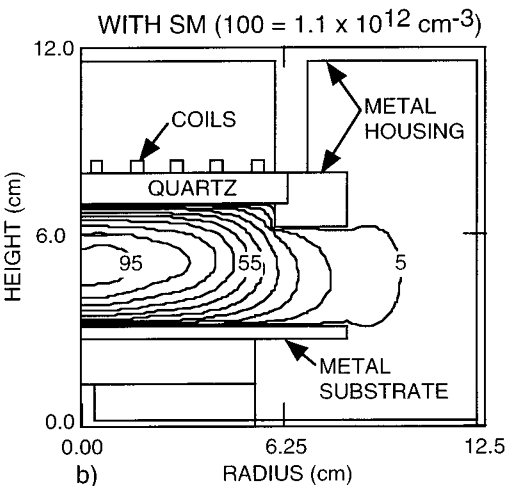

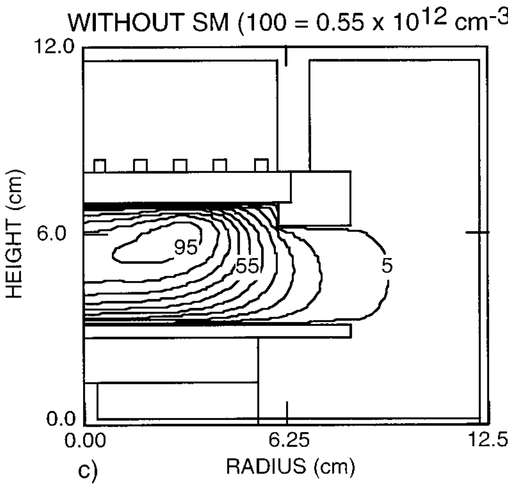

FIG. 3. Comparison of predicted electron density (10 mTorr Ar, 245 W) with experiments (see Ref. 19). (a) $[e]$ as a function of radius at midplane. The model results are normalized to the experiment. (b) Predicted $[e]$ with the SM. (c) Predicted $[e]$ without the SM. When using the SM, the electron density peaks on axis. Contours are labeled with the percent of the maximum value shown at the top of the figure.

window. The wafer-to-window distance is 7.5 cm. The wafer diameter is 20 cm, and is surrounded by an alumina focus ring. The wafer is treated as a uniform disk with a conductivity of 0.05 $(\Omega\ \mathrm{cm})^{-1}$. The coils are driven at 13.56 MHz.

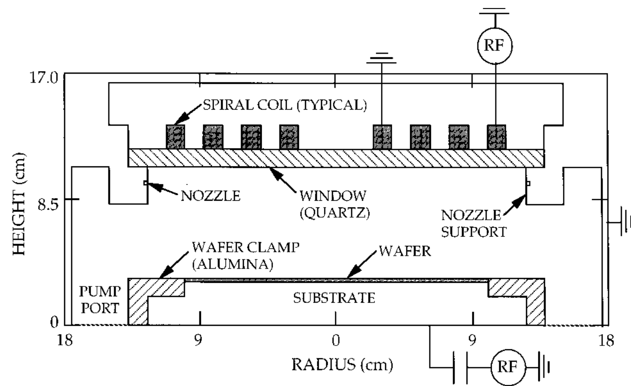

FIG. 4. Schematic of the ICP reactor used in this study.

The gas is Ar at 10 mTorr with an inlet flow rate of 100 sccm. The coils deliver 400 W of inductively coupled power to the plasma. The wafer is biased at 13.56 MHz with 200 W of power deposition (32 V bias voltage amplitude).

To demonstrate the effect of the SM on plasma parameters when using rf biases, cases were also run without the SM having the same bias power, and without the SM having the same applied voltage to compare to the standard case. The electron densities for these three cases are shown in Fig. 5. The ionization is maximum in a torous at approximately half the radius located a few cm below the dielectric window.[21] It is in this region that the power deposition is at a maximum due to the finite skin depth of the inductively

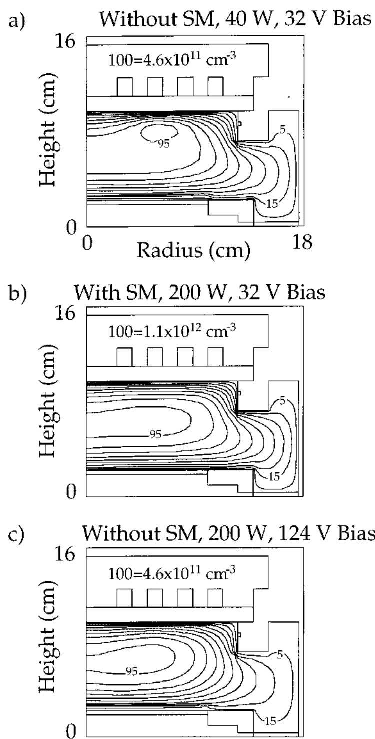

FIG. 5. Electron density for an inductively coupled Ar plasma at 10 mTorr and 400 W ICP power, (a) without the SM and 32 V rf bias voltage, (b) with the SM and 200 W rf bias power, and (c) without the SM and 200 W rf bias power. The contours are labeled with the percentage of the maximum value shown at the top of each figure.

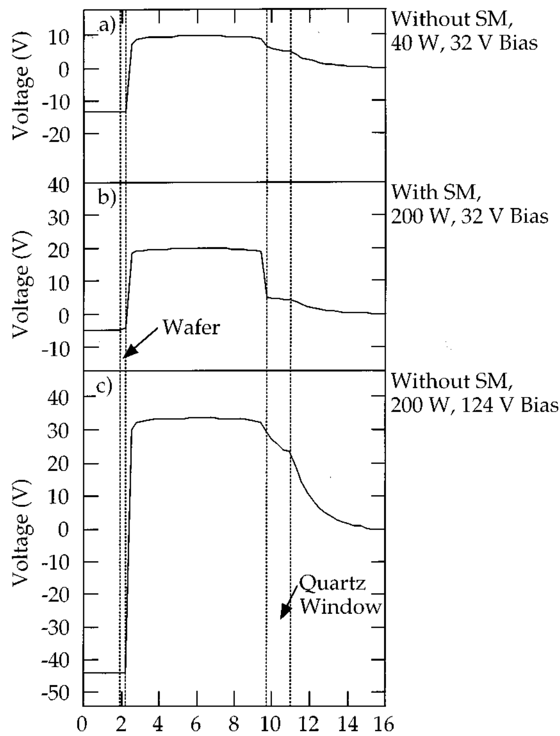

FIG. 6. Time averaged electric potential at the $r=0$ axis as a function of height. (a) without the SM and 32 V rf bias voltage, (b) with the SM and 200 W rf bias power, and (c) without the SM and 200 W rf capacitive power.

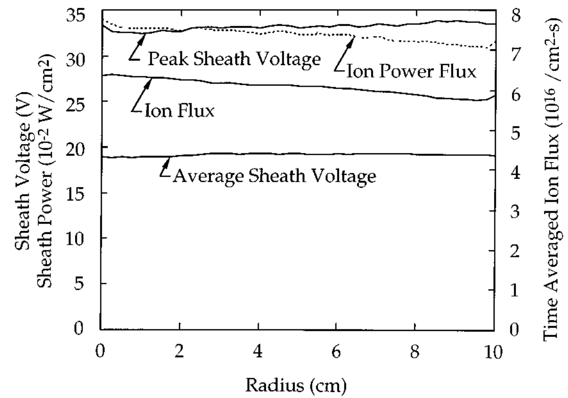

FIG. 7. Time averaged ion flux to the wafer, peak, and time averaged magnitude of the sheath voltage, and ion power flux as a function of radius across the wafer. The sheath potential is quite uniform across the wafer. As a result, the ion power scales with the ion flux.

coupled electric field into the plasma. The electrons produced in this region diffuse under ambipolar forces to the walls. The electron density for the case without the SM but with the same bias voltage on the substrate [Fig. 5(a)] has a profile which is sharply peaked near the source region with a maximum value of 4.6×10^{11} cm^{-3}. The plasma potential is also peaked off axis. When using the SM [Fig. 5(b)], a larger fraction of the plasma potential is dropped across the sheath as compared to the bulk. As a result, the plasma potential is flatter in the bulk. The rate of loss of electrons to the wall and through the sheath from a mean-free-path away is reduced since the sheath potential is higher. The electron density with the SM has a maximum value of 1.1×10^{12} cm^{-3}, both higher and more uniform than in the absence of the sheath model, both a consequence of the redistributed plasma potential. The general experimental observation for these conditions is that there is not a large off axis maximum in electron density. These same trends were observed in the simulations of IC-GECRC discussed in Sec. III. The SM therefore appears to provide boundary conditions in the FKS which generate more physical solutions. The case without the SM but with the same rf bias power as the case with the SM [Fig. 5(c)] has the same peak electron density as the case without the SM and with the same bias power. The bias voltage for this case is somewhat larger (124 V) to obtain the same bias power as the case with the SM because the ion flux to the wafer is smaller. As a result, the electron density is somewhat more uniform. For these conditions, we have empirically found that plasma uniformity improves with increasing bias voltage.

The cycle averaged plasma potential as a function of height at $r=0$ is shown in Fig. 6 for the same conditions as in Fig. 5. Examining the cases with and without the SM and which have the same applied bias voltage, we see that the total voltage drop between the bulk plasma and the powered electrode is nearly the same, 23–25 V. This correspondence is a consequence of the fact that the ion and electron currents to the surface must be equal since the wafer has a low conductivity and it is capacitively coupled to the power source. The dc bias, however, is smaller (less negative) for the case with the SM. This is a direct consequence of the plasma density being larger with the SM. It has been experimentally observed that for the same bias rf voltage amplitude, the dc bias decreases (becomes less negative) with increasing coil power and plasma density. These trends are discussed in more detail in Ref. 21. Comparing the cases with and without the sheath model at the same deposited power are more difficult, since a larger applied voltage (124 V) is required to obtain the same bias power without the SM. This results from the fact that the ion flux is higher when the SM is used, and therefore a smaller applied bias voltage is required to obtain the same power deposition. The larger rf bias voltage produces a larger (more negative) dc bias.

The cycle averaged ion flux to the wafer, the cycle averaged and peak sheath voltage, and the ion power density as a function of radius across the wafer are shown in Fig. 7 for the conditions of Fig. 5 with the SM. For this reactor configuration, the sheath voltage is fairly uniform across the wafer with a time averaged value of 19 V and a peak value of about 34 V. The ion flux is also fairly uniform, although it is slightly larger near the center of the wafer, 6.4×10^{16} cm^{-2} s^{-1} compared to 5.8×10^{16} cm^{-2} s^{-1} at the outer edge. The ion power density to the surface follows the ion flux ranging between 0.31 and 0.34 W/cm^2. Ions gain energy crossing the sheath potential, whose potential is relatively uniform as a function of radius. The radial dependence of the ion power flux to the wafer will therefore simply scale with radial dependence of the ion flux. This is the desired mode of operation.

The sheath voltage and sheath thickness above the wafer at the half-radius location are shown in Fig. 8 as a function

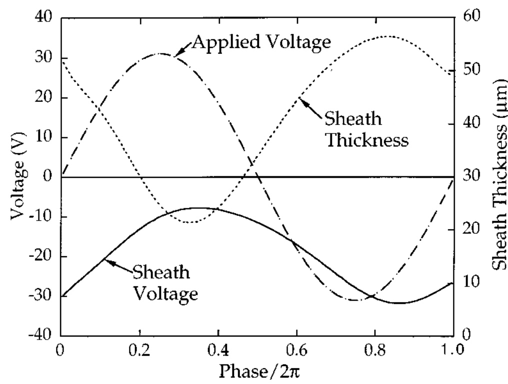

FIG. 8. Sheath voltage and thickness above the wafer at the half radius location ($r=5$ cm) as a function of rf phase. The applied voltage waveform is included for comparison.

of rf phase for the conditions of Fig. 7. The sheath voltage is defined with respect to the plasma potential, and is therefore negative. As the applied voltage becomes more positive, the plasma potential increases and therefore the sheath potential at unbiased surfaces increases to maintain the electropositive nature of the plasma. This forces electrons toward the powered electrode, reducing Q in the sheath, which in turn reduces the magnitude of the sheath potential on the powered electrode. As the applied voltage decreases, the plasma potential decreases. Since it must also float above the grounded electrode, the electrons are forced away from the powered electrode, increasing Q, and increasing the magnitude of the sheath potential above the wafer. Since only moderate voltages are applied, in this case an amplitude of 32 V rf, the sheath voltage remains nearly sinusoidal, and is nearly in phase with the driving voltage. The sheath voltage lags the applied voltage by approximately 45° due to the large capacitance of the sheath. The sheath thickness ranges from a minimum of 20 μm to a maximum of 57 μm and for the most part follows the magnitude of the sheath voltage. Its deviation from being sinusoidal results from modulation of the charged particle densities at the edge of the sheath during the rf phase.

One of the important motivations for using an inductively coupled plasma source with substrate biasing is to be able to separately control the magnitude, uniformity, and energy of the ion flux to the wafer. The peak flux to the wafer and the uniformity across the wafer for a variety of operating conditions in Argon are shown in Fig. 9. The nonuniformity in the ion flux, is defined as $(Max-Min)/\frac{1}{2}(Max+Min)$ $\times 100\%$. With 400 W of ICP power, the magnitude of the ion flux to the surface does not vary greatly as the rf bias power is increased by increasing the bias voltage [Fig. 9(a)]. The ion flux remains near 6×10^{16} cm^{-2} s^{-1}. The nonuniformity decreases from 20% to 3% when increasing the substrate power and rf bias voltage. We find that larger rf biases produce more uniform ion fluxes when bias power becomes comparable with ICP power and the discharge current resembles that of a capacitive discharge. For moderate rf bias power, the nonuniformity is relatively insensitive to the rf bias power.[22] The small increase in average ion flux obtained when applying the bias is more a consequence of the improved uniformity than an absolute increase in flux. The effects of varying ICP power on ion flux and nonuniformity are shown in Fig. 9(b). The results are somewhat different depending upon whether the bias voltage or power are held constant. The uniformity improves with increasing ICP power when the voltage is fixed. This is due in part to the fact that as the plasma density increases the bias power increases, and remains comparable to the ICP power. A more interesting result is obtained when the capacitively coupled power deposition is held constant while the inductive power

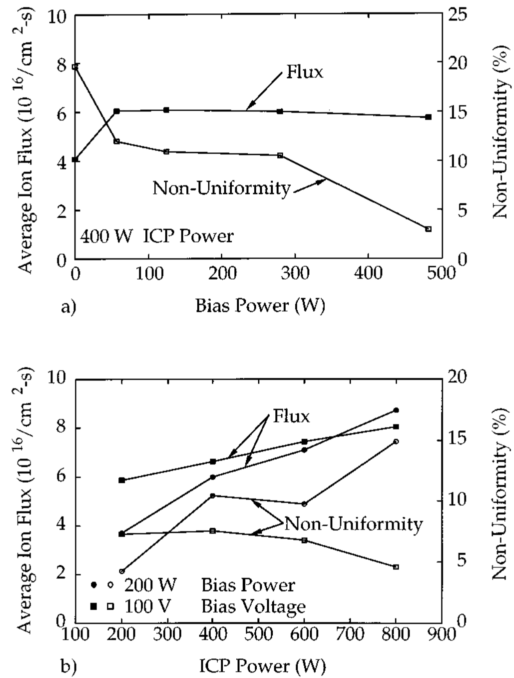

FIG. 9. Mean value of the time averaged ion flux to the wafer and the nonuniformity of the ion flux, defined as $(Max-Min)/\frac{1}{2}(Max+Min)$. (a) 400 W ICP power as a function of rf bias power, (b) 200 W rf capacitive power (open symbols) and 100 V rf applied voltage (solid symbols) as a function of ICP power. In general, ion flux uniformity improves with increasing bias voltage.

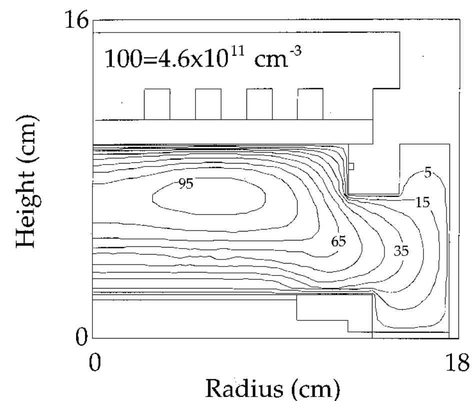

FIG. 10. Electron density for an Ar/Cl_2 discharge at 10 mTorr with 400 W ICP power and 100 V rf applied voltage on the substrate. The plasma is less uniform than the argon only case due to the increased collisionality of the Ar/Cl_2 gas mixture. The contours are labeled with the percentage of the maximum value shown at the top of each figure.

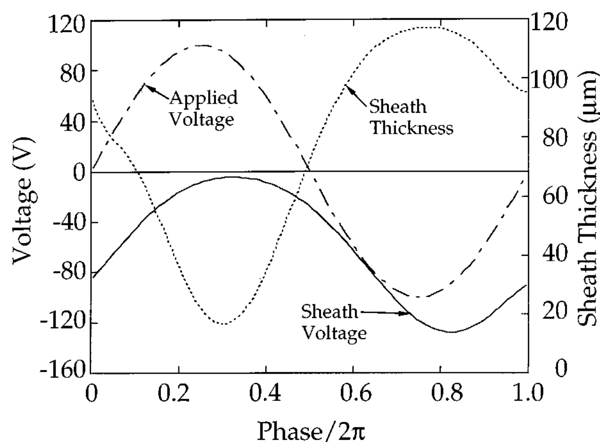

FIG. 11. Sheath voltage and thickness above the wafer at the half-radius location ($r = 5$ cm) as a function of rf phase for the Ar/Cl_2 discharge. The applied voltage wave form is included for comparison. The sheath thickness is less sinusoidal compared to the argon only case.

deposition is increased. In this case, the applied rf bias voltage required to obtain the same bias power decreases, which can cause a decrease in uniformity.

The sheath model can also be applied to plasmas having multiple ion species. As an illustration, the model was run for an Ar/Cl_2 plasma with an inlet flow rate of 50 sccm for each gas. The inductively coupled power deposition was 200 W, and a 100 V rf was applied to the substrate. The electron density for this case is shown in Fig. 10 and has a peak plasma density of 4.6×10^{11} cm^{-3}. The Ar/Cl_2 plasma is peaked off axis where the electron source is located and is less uniform than the pure Ar case due to the increased collisionality of the gas mixture and the large Cl^- density.

The sheath thickness and voltage as a function of rf phase for the Ar/Cl_2 case are shown in Fig. 11. The results are qualitatively the same as for the Ar only case (Fig. 8). For otherwise similar operating conditions, electronegative plasmas can have thinner sheaths. However in this example, the sheath is thicker than the Ar plasma due to the lower plasma density and the larger sheath potential. The sheath thickness is also less sinusoidal appearing somewhat more resistive compared to the argon only case, a consequence of perturbation of the electron flux entering the sheath produced by the presence of the negative ions.

The average ion flux to the wafer for the Ar/Cl_2 case is shown in Fig. 12. Results are shown for an rf bias of 100 V as a function of ICP power and for 400 W ICP power as a function of the bias voltage. With 400 W of ICP power, the magnitude of the ion flux to the surface rises slightly as the voltage is increased reaching a value near 6×10^{16} cm^{-2} s^{-1} at larger voltages. This trend results primarily from an improvement in plasma uniformity. When the applied bias voltage is held constant, the magnitude of the ion flux increases as the ICP power increases, as expected, since the plasma density depends primarily on the inductively coupled power. From these results, we see that the ion flux to the wafer is a function of both the rf bias and the inductively coupled power, with a stronger dependence on the inductively coupled power.

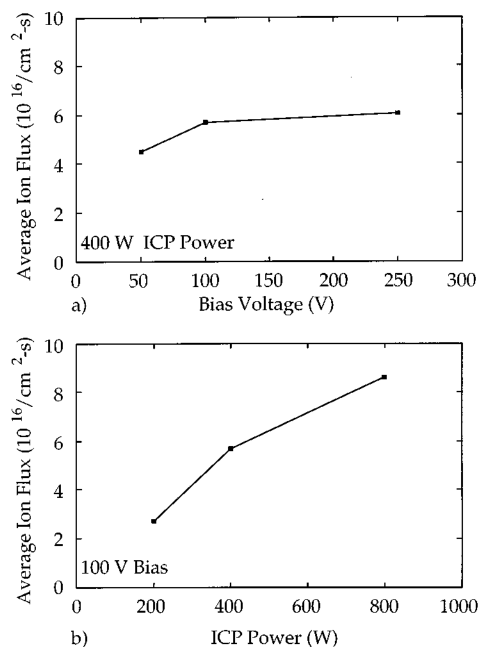

FIG. 12. Mean value of the time averaged ion flux to the wafer for the Ar/Cl_2 discharge for (a) 400 W ICP power as a function of bias voltage, and (b) 100 V rf bias voltage as a function of ICP power.

V. CONCLUDING REMARKS

Properly representing the rf sheath in models of high plasma density tools is important to correctly predict the plasma density and potential. In implementing a semianalytic sheath model into a two-dimensional model for rf biased ICP reactors, we found that predictions for the ion fluxes, power deposition, and the overall electrical characteristics of the plasma were affected. For example, incorporating the SM generally results in more uniform plasmas of higher electron density. In the cases, we investigated for plasma properties without an rf bias, agreement with experiment was more satisfactory than without the SM. We found that the sheath potential above the wafer was generally quite uniform as a function of radius, and so the radial dependence of the ion power flux depended primarily on the ion flux. We also found that the uniformity of the ion flux to the wafer generally improved with increasing rf bias, a consequence of flattening the time averaged plasma potential.

ACKNOWLEDGMENTS

This work was supported by the Semiconductor Research Corporation, National Science Foundation (ECS 94-04133, CTS 94-12565), LAM Research Corporation, and the University of Wisconsin Engineering Research Center for Plasma Aided Manufacturing.

[1] J. Hopwood, Plasma Sources Sci. Technol. **1**, 109 (1992).
[2] M. S. Barnes, J. C. Foster, and J. H. Keller, Appl. Phys. Lett. **62**, 2622 (1993).
[3] J. H. Keller, J. C. Foster, and M. S. Barnes, J. Vac. Sci. Technol. A **11**, 2487 (1993).
[4] R. Patric, R. Schoenborn, and H. Toda, J. Vac. Sci. Technol. A **11**, 1296 (1993).
[5] J. B. Carter, J. P. Holland, E. Peltzer, B. Richardson, E. Bogle, H. T.

Nguyen, Y. Melaku, D. Gates, and M. Ben-Dor, J. Vac. Sci. Technol. A **11**, 1301 (1993).
[6] W. Z. Collison and M. J. Kushner, Appl. Phys. Lett. **68**, 903 (1996).
[7] M. A. Lieberman, Trans. Plasma Sci. **16**, 638 (1988).
[8] V. A. Godyak and N. Sternberg, Trans. Plasma Sci. **18**, 159 (1990).
[9] N. Sternberg and V. A. Godyak, Trans. Mag. **30**, 3100 (1994).
[10] K. Börnig, Appl. Phys. Lett. **60**, 1553 (1992).
[11] M. A. Lieberman, Trans. Plasma Sci. **17**, 338 (1989).
[12] A. Metze, D. W. Ernie, and H. J. Oskam, J. Appl. Phys. **60**, 3081 (1986).
[13] M. E. Riley, Sandia Report SAND95-0775.UC-401 (1995).
[14] V. A. Godyak and N. Sternberg, Phys. Rev. A **42**, 2299 (1990).
[15] R. Farouki and M. Dalvie, J. Appl. Phys. **68**, 6106 (1990).
[16] Y. Wang, Appl. Phys. Lett. **66**, 2329 (1995).
[17] T. E. Nitschke and D. B. Graves, Trans. Plasma Sci. **23**, 717 (1995).
[18] M. J. Kushner, W. Z. Collison, M. J. Grapperhaus, J. P. Holland, and M. S. Barnes, J. Appl. Phys. **80**, 1337 (1996).
[19] A. J. Lichtenberg, V. Vahedi, and M. A. Lieberman, J. Appl. Phys. **75**, 2339 (1994).
[20] P. A. Miller, G. A. Hebner, K. E. Greenberg, P. D. Pochan, and B. P. Aragon, J. Res. Natl. Inst. Stand. Technol. **100**, 427 (1995).
[21] P. L. G. Ventzek, M. J. Grapperhaus, and M. J. Kushner, J. Vac. Sci. Technol. B **12**, 3118 (1994).
[22] R. Hill, J. Vac. Sci. Technol. B **14**, 547 (1996).